ACS OMEGA

http://pubs.acs.org/journal/acsodf

Article

Electrochemical Reduction and Oxidation of Chlorinated Aromatic Compounds Enhanced by the Fe-ZSM-5 Catalyst: Kinetics and Mechanisms

Yuexuan Li, Yun Liu,* Xuan Zhang, Kun Tian, Ding Tan, Xiaosan Song, Ping Wang, Qian Jiang, and Junhe Lu

Cite This: *ACS Omega* 2022, 7, 33500−33510

Read Online

ACCESS | Metrics & More | Article Recommendations | Supporting Information

ABSTRACT: Devising cost-effective electrochemical catalyst system for the efficient degradation of chlorinated aromatic compounds is urgently needed for environmental pollution control. Herein, a Fe-ZSM-5 zeolite was used as a suspended catalyst to facilitate the degradation of lindane as a model chlorinated pesticide in an electrochemical system consisting of the commercial DSA (Ti/RuO_2-IrO_2) anode and graphite cathode. It was found that the Fe-ZSM-5 zeolite greatly accelerated the degradation of lindane, with the degradation rate constant more than 8 times higher than that without Fe-ZSM-5. In addition, the Fe-ZSM-5 zeolite widened the working pH range from 3 to 11, while efficient degradation of lindane in the absence of Fe-ZSM-5 was only obtained at pH ≤ 5. The degradation of lindane was primarily due to reductive dechlorination mediated by atomic H* followed by •OH oxidation. Fe-ZSM-5 zeolite could enrich lindane, H*, and •OH on its surface, thus provided a suitable local environment for lindane degradation. The Fe-ZSM-5 zeolite exhibited high stability and reusability, and reduced the energy consumption. This research provides a potential reduction−oxidation strategy for removing organochlorine compounds through a cost-efficient Fe-ZSM-5 catalytic electrochemical system.

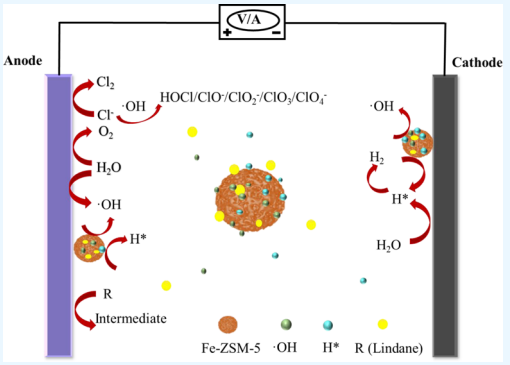

1. INTRODUCTION

Chlorinated aromatic compounds such as insecticides, herbicides, and pharmaceuticals have been widely detected in the environment as they have been widely used over the past decades.[1,2] These chemicals usually have strong biotoxicity, bioaccumulation, and teratogenic mutagenicity.[3] Lindane (γ-hexachlorocyclohexane), a representative organochlorine pesticide, has been widely used in agricultural, veterinary, and human applications between the 1940s and 1990s.[4,5] Although lindane has been banned in many countries, it is still widely detected in surface waters, groundwaters and soils because of a large number of applications in the past.[6,7] Due to its refractoriness and potential hazardous risk, lindane was included in the Stockholm Convention as a persistent organic pollutant and challenging to remove from the environment. Therefore, highly effective remediation technologies are urgently required for this kind of chlorinated aromatic pollutants.

Although the intrinsic characteristics of the molecule, several techniques including incineration,[8] microbial dehalogenation,[9] and chemical oxidation[10] have been used for chlorinated aromatic compound degradation in waters or soils. Chemical oxidation with radical pathways, especially hydroxyl radicals (•OH), is frequently reported for the oxidation of lindane.[10] •OH could be generated by ozonation, photocatalytic reaction, Fenton reaction, and plasma oxidation.[11] Fenton processes caused decomposition of H_2O_2 to •OH catalyzed by Fe^{2+}/Fe^{3+} but were strongly dependent on pH. The photo-Fenton process was another way to generate •OH but also required strict pH control.[11] The electro-Fenton process is one of the most powerful methods for H_2O_2 generation.[12,13] The process still requires acidic pH conditions (i.e., pH 2.8−3.5).[14] Moreover, it generates a lot of iron-containing sludge.[15] Heterogeneous electro-Fenton processes can widen the operational pH range.[16] H_2O_2 would be transformed to •OH on the surface of the catalyst in the heterogeneous electro-Fenton process. The catalysts include iron minerals, iron-supporting materials, nanoparticles, and modified cathodic materials.[17] Among them, iron- and iron oxide-loaded materials such as layered double hydroxide containing Cu and Fe, Y−Fe,[18] zeolite catalyst,[19] Fe-clay,[20] and magnetic

Received: July 14, 2022
Accepted: August 31, 2022
Published: September 10, 2022

single-walled carbon nanotubes[21] have been proven to be efficient catalysts.[17]

Chemical reduction of chlorinated aromatic compounds has also been explored largely by reducing agents such as zero-valent iron,[22,23] bimetallic Fe-based nanoparticles,[24] and natural reducing agents.[25] The atomic H* can realize the dechlorination of lindane[26−29] and can be generated on noble metals in an electrochemical system to dechlorinate chlorinated organic compounds.[30−32] Palladium was the most favorable catalyst for its excellent capability in retaining H*.[30,33] However, the poor dispersibility and high cost of Pd metals limit its application.[31] Although H* could initiate dechlorination, the reaction could not continue readily for the high energy required.[26]

It was found that the coexistence of H* and •OH could decrease energy consumption and increase the degradation efficiency of pollutants.[26,34] Such synchronous reduction−oxidation systems have been constructed using a Pd-loaded $Cu/Cu_2O/CuO$ electrode,[26] a CoNi anchored on the ionic liquid functionalized graphene electrode,[34] and a Pd/graphene oxide hybrid fabricated on carbon fiber paper.[29] H* and •OH are generated through the hydrogen evolution reaction (HER), oxygen evolution reaction (OER), and oxygen reduction reaction (ORR) in electrochemical systems.[35,36] Boron-doped diamond (BDD) as a promising electrode material, has excellent properties for generation H* and •OH.[37,38] However, noble metals and BDD electrodes are more expensive than ruthenium oxide and/or iridium oxide layers based on dimensionally stable anodes (DSAs) and graphite electrodes.[39] DSAs and graphite electrodes are widely explored to remove organic compounds and generally are used in industrial electrochemical processes.[40−44] Thus, there will be a great need to use these commercial electrodes for industrial applications if H* and •OH could be simultaneously generated in such electrochemical systems.

Electrocatalysts have been proven to affect the rate of chemical reactions and promote the generation of active species.[45] Powder-activated carbon loaded with metallic cobalt (Co) could catalytically generate both H* and •OH in a three-dimensional electrocatalytic system.[29,46] Pd/Al_2O_3 particles provided a large surface area for atomic H* production, which was responsible for Fe^{3+} reduction to Fe^{2+}.[47] Nowadays, transition metals such as Fe, Co, Ni, Cu, and Mn exhibit efficient catalytic activity for electrochemical reactions which are cheaper and easier to obtain than noble metals.[26,46,48] Metal oxide-based materials such as TiO_2, Ti_2O_3, and MnO_2 also served as efficient HER electrocatalysts associated with H* adsorption/desorption via either Volmer−Heyrovsky or Volmer−Tafel mechanisms.[49] Fe-ZSM-5 zeolites have been widely explored in the heterogeneous Fenton process due to their highly catalytic ability,[50−56] which have a potential for industrialization.[57] Thus, it is significant to explore cost-efficient materials as electrocatalytic particles to degrade organochlorine compounds.

The main objective of this paper is to promote the usage of atomic H* and •OH for the effective degradation of lindane by Fe-ZSM-5 particles. Lindane was selected as a model of chlorinated aromatic compounds. The degradation of lindane was performed in a heterogeneous catalytic electrochemical system over the Fe-ZSM-5 zeolite catalyst using commercially available electrodes. The effects of current density, solution pH, and amounts of Fe-ZSM-5 catalysts on the lindane degradation were studied. The energy consumption and catalyst reusability were studied as well.

2. MATERIALS AND METHODS

2.1. Chemicals and Materials. ZSM-5 zeolites with Si/Al ratios of 25 were supplied by Tianjin Nankai University Catalyst Co., Ltd. Lindane (97%), 5,5-dimethyl-1-pyrroline *N*-oxide (DMPO), isopropyl alcohol (IPA), tert-butanol (TBA), and 1,4-benzoquinone (PBQ) were obtained from Sigma-Aldrich. Other chemicals were purchased from Sinopharm.

2.2. Preparation and Characterization of Fe-ZSM-5 Zeolites. The Fe-ZSM-5 catalyst was synthesized according to the previous work with a minor modification.[58] In brief, ZSM-5 zeolites (200 g) were impregnated with $Fe(NO_3)_3$ aqueous solution (17.8 g $Fe(NO_3)_3{\cdot}9H_2O$), and the mixture was stirred for 4 h and then evaporated at 70 °C. Then, the samples were calcined for 4 h at 550 °C in a muffle furnace to obtain Fe-ZSM-5 zeolites. The Fe elements on the surface of Fe-ZSM-5 were characterized by using an ESCALAB 250Xi spectrometer (Thermo Scientific, USA). After Fe-ZSM-5 was degassed at 120 °C for 12 h, the surface area and porosity of Fe-ZSM-5 zeolites were characterized by N_2 adsorption−desorption isotherms measured on an ASAP2010 Accelerated Surface Area and Porosimetry Adsorption Analyzer (Micromeritics). The surface morphology and elements of Fe-ZSM-5 zeolites were observed using a LEO 1530 VP scanning electron microscope at the Nanjing Institute of Geology and Paleontology. The XRD patterns (SmartLab 9, Rigaku Corporation in Japan) of Fe-ZSM-5 were detected at a scan rate of 2° min^{-1} under 40 kV and 150 mA. UV−vis diffuse reflectance spectroscopy (UV−vis DRS) of Fe-ZSM-5 was obtained using a UV−vis−NIR 3600 Plus spectrophotometer (Shimadzu Corporation, Kyoto, Japan).

2.3. Electrochemical Experiments. Electrochemical experiments were performed in a cylindrical glass reactor (150 mL) with screw caps working with magnetic stirring. A graphite plate cathode (2.5 cm × 2 cm × 1 mm) was purchased from Qingdao Baofeng Graphite Corporation, and a DSA (mixed metal oxide, Ti/RuO_2-IrO_2) anode (2.5 cm × 2 cm × 1 mm) was purchased from Yiwanlin Electronics Technology Corporation. A sodium sulfate aqueous solution (3 g/L) was used as the supporting electrolyte according to the previous work.[59]

The effects of current density (from 6 to 30 mA/cm^2), initial pH (from 3 to 11 adjusted by HCl or NaOH), and doses of Fe-ZSM-5 zeolites (from 0.1 to 1.0 g/L) on the lindane degradation process were studied. 0.5 mL samples were taken off from the reaction solution with magnetic stirring at specific times and mixed with 1 mL *n*-hexane, and the extract was measured by gas chromatography with an electron capture detector (GC-ECD). Scavenging experiments were conducted by different scavengers (IPA, TBA, and PBQ) to estimate the role of reactive radicals. The degradation intermediate solution was collected at 5 min, 10 min, 30 min, 1 h, 2 h, 4 h, and 8 h and mixed together. The mixture was extracted with *n*-hexane and was ready for gas chromatography/mass spectrometry (GC−MS). To study the dechlorination of lindane, the initial concentration of 5 mg/L was selected, and Cl^- concentrations were detected using Thermo Scientific Dionex Aquion Ion. The adsorption−desorption of lindane onto Fe-ZSM-5 was also studied, and a detailed procedure is shown in the Supporting Information. All the experiments were performed in triplicate.

https://doi.org/10.1021/acsomega.2c04458
ACS Omega 2022, 7, 33500−33510

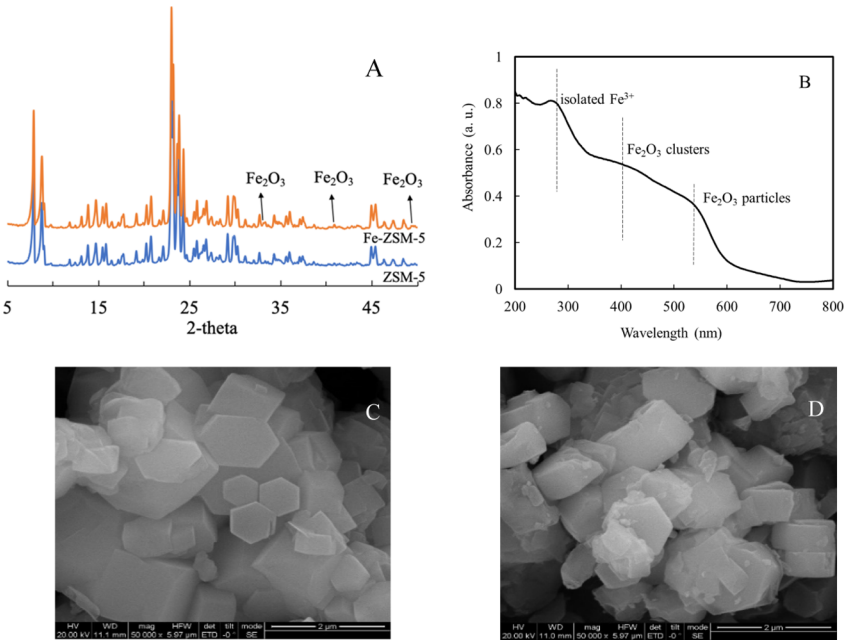

Figure 1. Characterization of ZSM-5 and Fe-ZSM-5. (A) XRD patterns of Fe-ZSM-5; (B) UV−vis diffuse reflectance spectroscopy of Fe-ZSM-5; (C) SEM morphology of ZSM-5; (D) SEM morphology of Fe-ZSM-5.

The degradation reactions of lindane were modeled using the first-order kinetic equation.[60−64]

$$\ln \frac{C_t}{C_0} = -kt \tag{1}$$

where C_0 and C_t are the initial and residual concentrations of lindane at a specific time t, respectively. k is the rate constant of the degradation reaction calculated from the slope of $\ln(C_t/C_0)$ versus time t.

2.4. Analytical Methods. Lindane concentration was measured by an Agilent 7890A GC-ECD equipped with a CP-Sil 8 CB column (30 m × 0.25 mm × 0.25 μm), and intermediates of lindane degradation were analyzed by GC−MS (TQ-8050, Shimadzu). Operating conditions are shown in the Supporting Information. Possible products were identified by retrieving the mass spectra in the NIST standard library. Total organic carbon (TOC) in the solution was detected by Analyzer multi N/C UV (Analytic Jena, Germany) according to the 800 °C combustion catalytic oxidation method. Electrochemical energy consumption (EEC) for TOC removal during electrolysis at a constant current was computed from experimental TOC versus time according to the following equations (eq 2).[13,25]

$$EC_{TOC} = \frac{UIt}{(\Delta TOC)_t V_s} \tag{2}$$

where U is the average cell voltage (V), I is the applied current (A), t is the electrolysis time (h), V is the solution volume (L), and ΔTOC is the experimental TOC decay (mg/L) reached at time t.

The electron paramagnetic resonance (EPR) signals of radicals trapped by DMPO were detected using an E500-9.5/12 EPR spectrometer. Detailed information is shown in the Supporting Information.

3. RESULTS AND DISCUSSION

3.1. Characterization of Fe-ZSM-5. Nitrogen sorption−desorption isotherms of Fe-ZSM-5 are shown in Figure S1A. Fe-ZSM-5 showed type I adsorption isotherms and type H4 hysteresis loops, suggesting a microporous property (Figure S1A), and the pore size distribution of Fe-ZSM-5 by applying the Horvath−Kawazoe model ranged from 0.50 to 0.98 nm (Figure S1B). The BET specific surface area and total pore volume of Fe-ZSM-5 were 403.6 m^2/g and 0.215 cm^3/g, respectively. The main pore size was 0.545 nm (Table S1). The XRD pattern of Fe-ZSM-5 showed typical diffraction peaks attributed to traditional ZSM-5 MFI topology (JCPDS: no. 49-0657), such as the peaks at 7.9, 8.8, 23.0, 23.2°, and so forth. Weak diffraction peaks (33.2, 40.9, and 49.5°) attributed to Fe_2O_3 (JCPDS: no. 033-0664) were also observed (Figure 1A). The XPS spectrum of Fe-ZSM-5 (Figure S1C) revealed the composition and chemical states of Fe on its surface. The binding energy peaks located around 711 and 724.7 eV in Fe-ZSM-5 corresponded to the Fe 2p3/2 and 2p1/2 states of iron in Fe_2O_3.[65,66] The spectrum of Fe 2p3/2 could be deconvoluted into two peaks at 710.9 and 713.6 eV.[65] The weak peak at 718.5 eV was related to the Fe^{3+} oxidation state.[65,66] Chemical states of Fe on the ZSM-5 surface were further confirmed by UV−vis diffuse reflectance spectroscopy of Fe-ZSM-5 (Figure 1B). An adsorption band at 545 nm appeared, showing the existence of Fe_2O_3 particles on the ZSM-5 surface,[67,68] and an apparent adsorption band at about 280 nm showing isolated octahedral Fe^{3+} complexes.[68,69] A weak band at about 400 nm was observed, showing an aggregation of Fe_2O_3 clusters.[68,70] The SEM morphology of ZSM-5 zeolite showed cube-like crystals with a smooth surface (Figure 1C), and the SEM morphology of Fe-ZSM-5 zeolite showed few Fe_2O_3 particles on the surface of ZSM-5 (Figure 1D). The EDS elemental percentage of ZSM-5 and Fe-ZSM-5 are shown in Table S2, and the appearance of Fe was observed on the Fe-ZSM-5 catalyst. Thus, Fe_2O_3 was formed on the surface of ZSM-5.

https://doi.org/10.1021/acsomega.2c04458
ACS Omega 2022, 7, 33500−33510

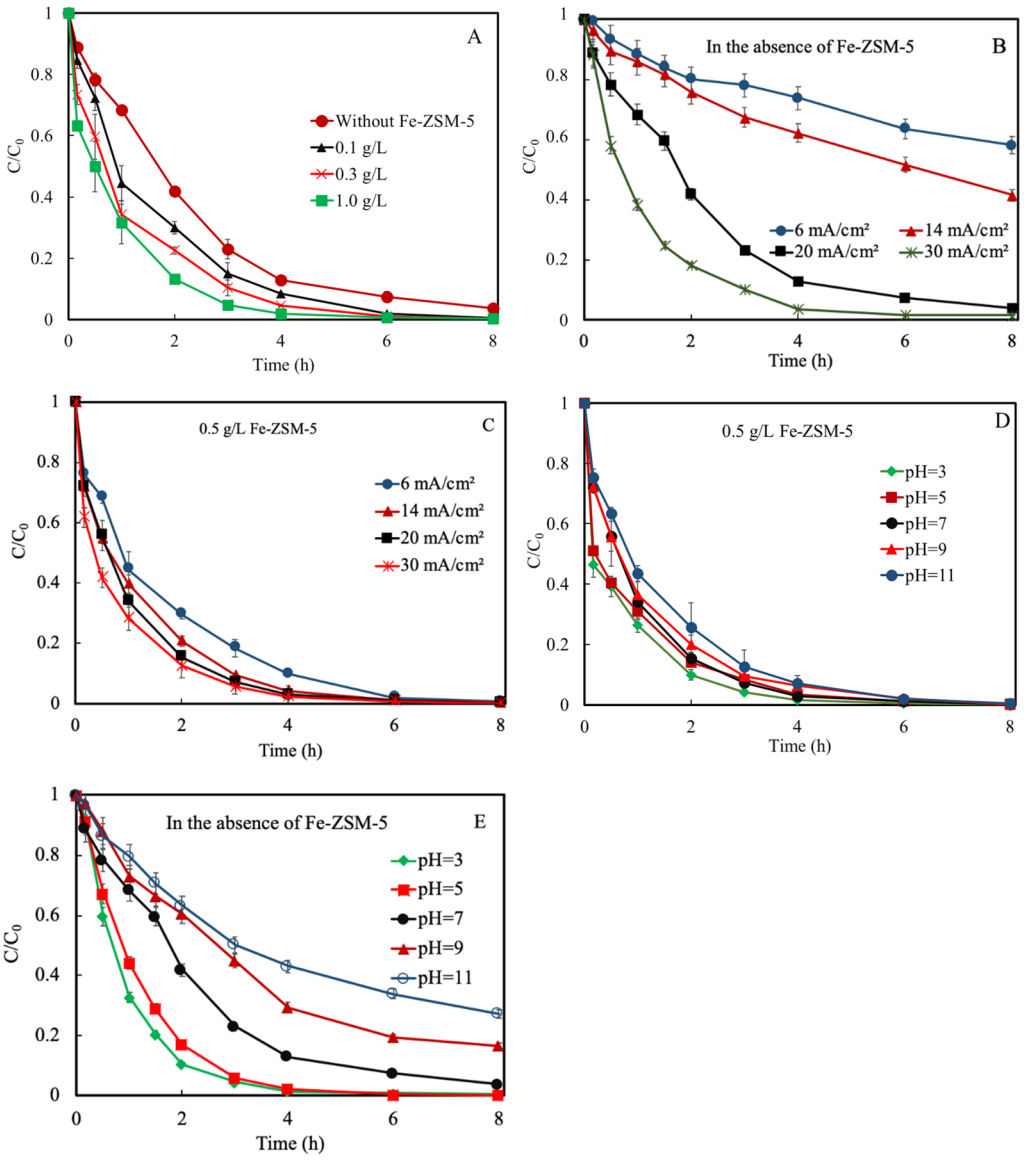

Figure 2. Degradation kinetics of lindane. (A) Doses of Fe-ZSM-5 ranging from 0.1 to 1.0 g/L at 20 mA/cm^2; (B) current density ranging from 6 to 30 mA/cm^2 without Fe-ZSM-5; (C) current density ranging from 6 to 30 mA/cm^2 with 0.5 g/L Fe-ZSM-5; (D) initial pH ranging from 3 to 11 with 0.5 g/L Fe-ZSM-5 at 20 mA/cm^2; (E) initial pH ranging from 3 to 11 without Fe-ZSM-5 at 20 mA/cm^2.

3.2. Lindane Degradation Kinetics. The degradation of lindane was conducted at different current densities, Fe-ZSM-5 doses, and initial pH values (Figure 2). Lindane degradation efficiencies of 58.2, 70.0, 77.4, 84.6, and 86.7% with free Fe-ZSM-5, 0.1, 0.3, 0.5, and 1.0 g/L Fe-ZSM-5, respectively, were achieved in 2 h (Figure 2). All the data can be well fitted with first-order kinetic model (Tables S3 and S4). The degradation of lindane increased with the increase of Fe-ZSM-5 dose (Figure 2A). When the Fe-ZSM-5 zeolite dose was increased from 0.1 to 1.0 g/L, the degradation rate constants increased from 0.6494 to 0.8343 h^{-1} (Table S3). When the Fe-ZSM-5 dose was over 0.5 g/L, no further apparent increase of the degradation rate constant was observed. The degradation rate constant with 0.5 g/L Fe-ZSM-5 (0.8284 h^{-1}) was close to that with 1.0 g/L Fe-ZSM-5 (0.8343 h^{-1}).

Lindane was also slowly degraded in the electrochemical oxidation system in the absence of Fe-ZSM-5 (Figure 2B). Lindane degradation in 2 h was 19.8, 24.1, 58.2, and 81.7% at the current densities of 6, 14, 20, and 30 mA/cm^2, respectively. Also, the degradation rate constant values at a current density from 6 to 30 mA/cm^2 were in the range of 0.0745 to 0.6367 h^{-1} (Table S4). Compared to the degradation in the absence of Fe-ZSM-5, lindane degradation was accelerated greatly in the presence of Fe-ZSM-5 zeolites (Figure 2C). The lindane degradation rate constant increased from 0.6230 to 0.8902 h^{-1} when the current density was increased from 6 to 30 mA/cm^2 (Table S3). The degradation rate constant (0.8902 h^{-1}) at a current density of 30 mA/cm^2 was not much higher than that at a low current density of 6 mA/cm^2 (0.6230 h^{-1}) with Fe-ZSM-5. At a current density of 6 mA/cm^2, lindane was almost completely degraded in 6 h in the presence of Fe-ZSM-5, while the degradation efficiency was less than 40% without Fe-ZSM-5. The degradation rate constant of lindane (0.6230 h^{-1}) with Fe-ZSM-5 was more than eight-fold higher than that (0.0745 h^{-1}) without Fe-ZSM-5 at 6 mA/cm^2, close to that (0.6367 h^{-1}) obtained at a current density of 30 mA/cm^2 in the absence Fe-ZSM-5. Thus, adding Fe-ZSM-5 to the electro-

https://doi.org/10.1021/acsomega.2c04458
ACS Omega 2022, 7, 33500−33510

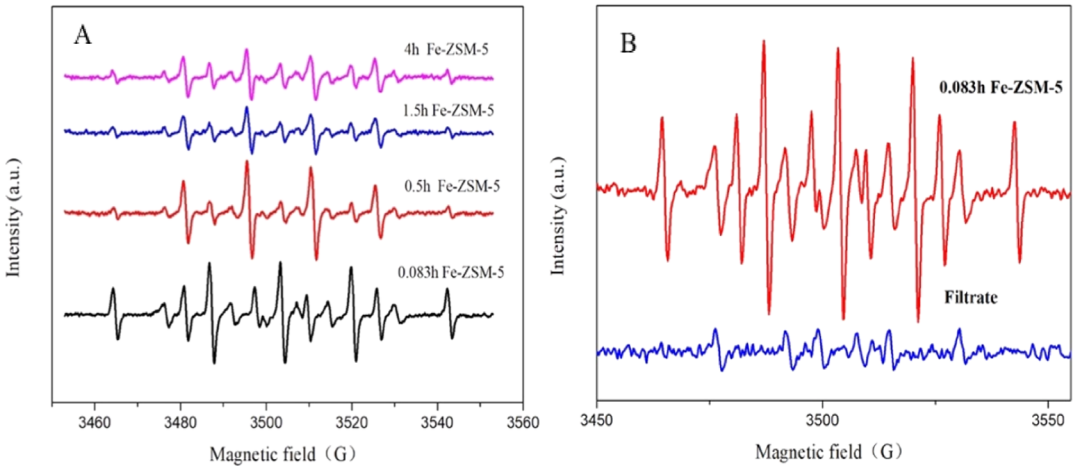

Figure 3. EPR spectra of radicals (A) at different reaction times ranging from 0.083 to 4 h; (B) in the filtrate and the solution containing Fe-ZSM-5 at 0.083 h.

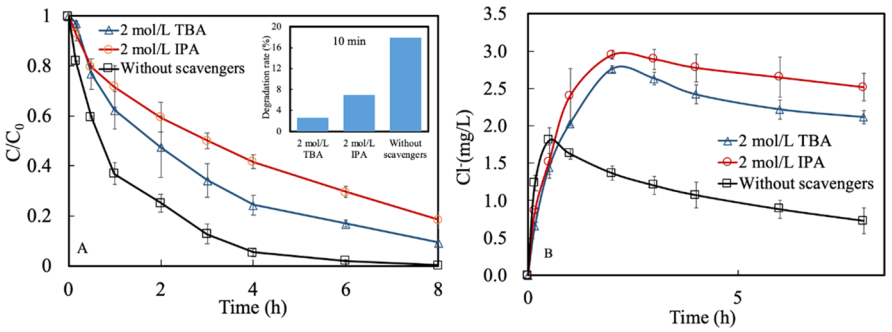

Figure 4. Effect of scavengers on lindane degradation. (A) A comparison of lindane degradation with scavengers and 0.5 g/L Fe-ZSM-5 at 20 mA/cm^2; (B) concentration of Cl^- during the degradation process with scavengers at 20 mA/cm^2 and 0.5 g/L Fe-ZSM-5.

chemical system can accelerate lindane degradation, especially at low current densities.

The effects of initial pH on lindane degradation with or without Fe-ZSM-5 are shown in Figure 2D,E. Lindane was effectively degraded with Fe-ZSM-5 over a pH range of 3−11, with the degradation rate constant ranging from 0.6825 to 0.9458 h^{-1} (Figure 2D). The degradation became slower with increasing pH regardless of the existence of Fe-ZSM-5 or not. In the absence of Fe-ZSM-5, a high degradation rate of lindane was only obtained at pH ≤ 5 (Figure 2E), and the degradation rate constant at pH 11 was only 0.1812 h^{-1}. Thus, the presence of Fe-ZSM-5 as an electrochemical catalyst can widen the working pH range. It is noted that the pH after 8 h was in the range of 2.89−4.22 when the initial pH was from 3 to 11 (Figure S2), suggesting the generation of acidic byproducts.

3.3. Identification of Active Radicals. To identify the radicals involved in the heterogeneous catalytic electrochemical process, EPR spectroscopic analysis was conducted with DMPO as the spin trap agent. The DMPO-H adduct characterized by nine peaks with a *g*-factor value of 2.00607 was evident at different reaction times (Figure 3A). The DMPO/$^{\bullet}$OH adduct characterized by four peaks (1:2:2:1) with a *g*-factor of 2.00625 was found at all the reaction times (Figure 3A), but the DMPO/$^{\bullet}O_2^-$ adduct (1:1:1:1 quartet) was not observed. At 5 min (0.083 h), the signal intensity of DMPO-H was stronger than that of DMPO/$^{\bullet}$OH. However, it shrank over time and became lower than that of DMPO/$^{\bullet}$OH after 30 min. Atomic H* can be generated by the electroreduction of H_2O or H^+.[71] Moreover, both atomic H* and $^{\bullet}$OH were adsorbed on the surface of Fe-ZSM-5 because characteristic peaks of DMPO-H and DMPO/$^{\bullet}$OH were not observed in the solution with Fe-ZSM-5 excluded, while the signals of DMPO-H and DMPO/$^{\bullet}$OH in the solution containing catalyst Fe-ZSM-5 were high (Figure 3B). The result indicated that Fe-ZSM-5 could enrich atomic H* and $^{\bullet}$OH.

3.4. Degradation Mechanisms and Pathways. The reactive $^{\bullet}$OH was usually regarded as the dominant oxidative species in the catalytic electrochemical systems, which could be scavenged by both IPA and TBA.[32] To evaluate the contribution of $^{\bullet}$OH to lindane degradation, IPA and TBA were added to the reaction solution as the radical scavengers. The degradation efficiency of lindane was apparently inhibited in the presence of IPA and TBA (Figure 4A), and the inhibition became more significant with the increase of the concentration of scavengers (Figure S3A,B). In the first 0.083 h, lindane degradation with IPA was higher than that with TBA at an equal concentration (Figure 4A). It is known that IPA reacts with $^{\bullet}$OH at a higher rate than TBA.[72,73] If $^{\bullet}$OH was the only species that was quenched, the result would be the opposite. Thus, there were other species responsible for lindane degradation in this study. Because H* was generated during the electrochemical process in this study (Figure 3B), and Mao et al. reported that TBA could react with H* rapidly, while H* could be formed because of water reduction in the cathode of the electrochemical reactor.[32] Therefore, it can be postulated that H* also contributed to lindane degradation,

https://doi.org/10.1021/acsomega.2c04458
ACS Omega 2022, 7, 33500−33510

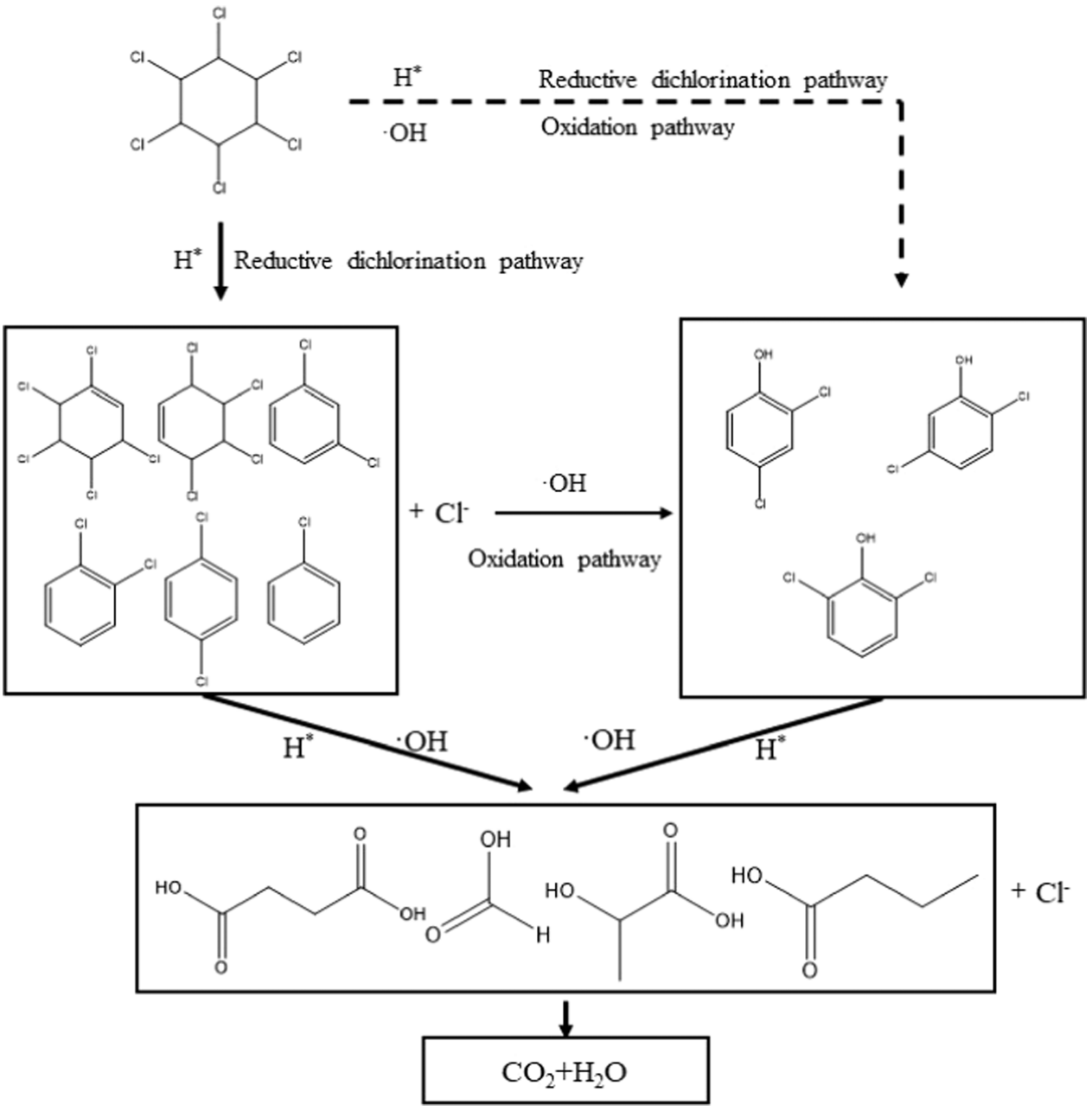

Figure 5. Proposed degradation mechanism of lindane.

especially during the earlier phase of the reaction. $HO_2^{\bullet}/O_2^{\bullet-}$ was another oxidative species that might exist in the catalytic electrochemical process. In this study, PBQ was applied to probe $HO_2^{\bullet}/O_2^{\bullet-}$. The results showed that the degradation rate of lindane was little affected by PBQ (Figure S3C), indicating that $HO_2^{\bullet}/O_2^{\bullet-}$, if formed, played a minor role in the degradation of lindane. Although with a high concentration of radical scavengers, lindane degradation was not completely suppressed (Figure 4A). This can be explained by the direct oxidation of the organic compounds through electron transfer on the anode. A similar result was observed: chlorinated hydrocarbons could be degraded through a direct oxidation pathway on anodes.[74,75]

To further explore the roles of H* and $^{\bullet}$OH, the concentrations of inorganic chlorine species during the degradation process were measured (Figure 4B). The time-course concentration of Cl^- showed a similar trend in the presence and absence of scavengers; that is, the concentration of Cl^- in the solution first increased and then decreased. This phenomenon is consistent with the results reported in the literature that dechlorination of lindane resulted in the formation of Cl^-, and Cl^- could be further oxidized to free chlorine and species with even higher oxidative states by $^{\bullet}$OH, such as ClO_2^-, ClO_3^-, and ClO_4^-, in electrochemical processes.[12,13,76] The concentration of Cl^- in the solution without scavengers was higher than those with scavengers in the first hour, which means that it was easy to dechlorinate lindane without scavengers. However, the concentration of Cl^- without scavengers was much lower than that with scavengers after 1 h. Both IPA and TBA can consume $^{\bullet}$OH, which would prevent the oxidation of Cl^- to a higher state.

Although the time-course concentration of Cl^- showed a similar trend in the presence of IPA or TBA, the concentration of Cl^- with TBA was lower than that with IPA in the whole

https://doi.org/10.1021/acsomega.2c04458
ACS Omega 2022, 7, 33500−33510

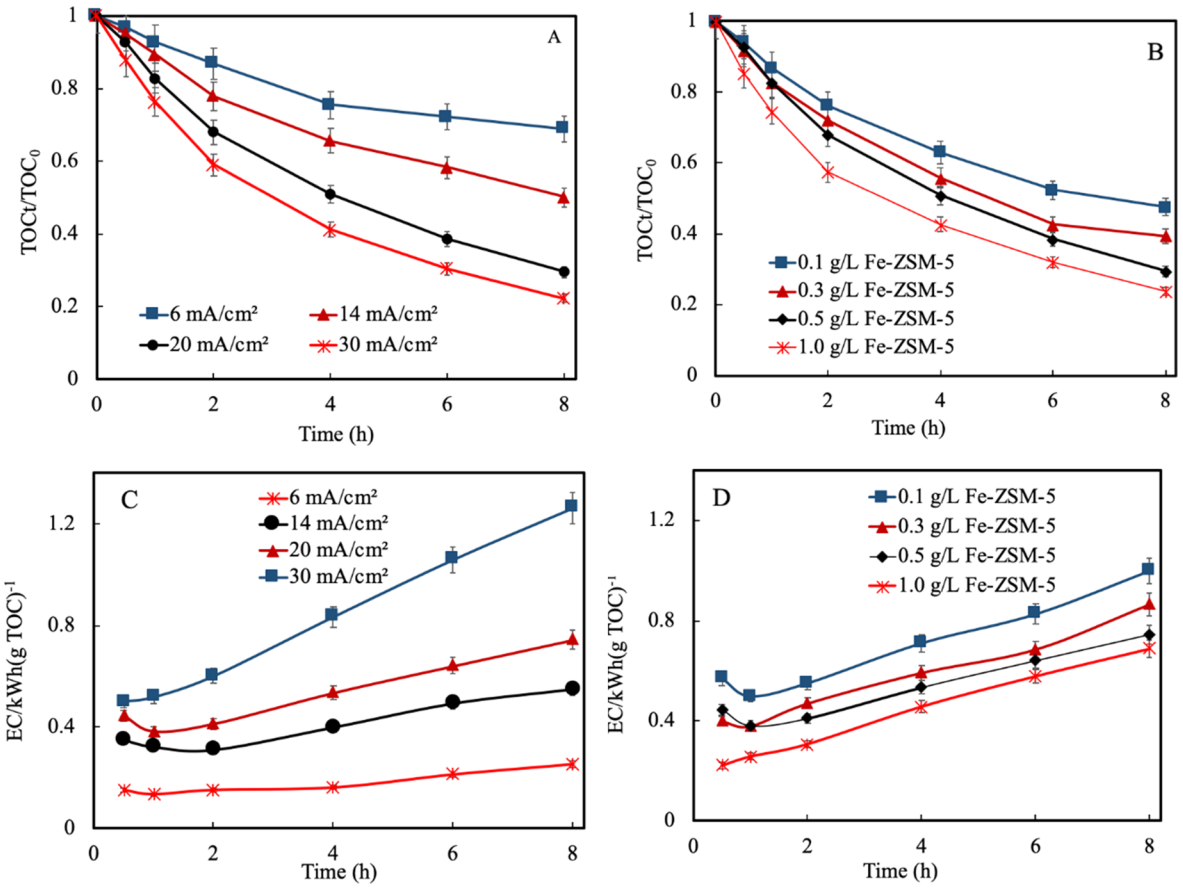

Figure 6. Mineralization of lindane and energy consumption in the presence of Fe-ZSM-5. (A) Effect of current density on lindane mineralization; (B) effect of dose of Fe-ZSM-5 on lindane mineralization; (C) effect of current density on the energy consumption; (D) effect of dose of Fe-ZSM-5 on the energy consumption.

reaction process (Figure 4B). As a reduction agent, H* caused lindane to dechlorinate and release Cl^-. TBA could consume H*, thus inhibiting reductive dechlorination of the targeted pollutant. As a result, Cl^- concentration with TBA was lower than that with IPA. Therefore, H* played an important role during lindane degradation. Lindane degradation in the presence of TBA was expected to be slower than that in the presence of IPA if H* acted as the primary reactive species governing lindane degradation. However, degradation of lindane with TBA was significantly faster than that with IPA after the first hour. This indicates that there were other reactive species contributing to lindane degradation, especially in the later reaction phase. Both IPA and TBA can quench $^{\bullet}OH$, but IPA reacts with $^{\bullet}OH$ more rapidly than TBA.[72] As a result, further transformation of Cl^- to other states by $^{\bullet}OH$ in the presence of IPA would be slower than that in the presence of an equal amount of TBA. More $^{\bullet}OH$ were consumed in the presence of IPA, which made lindane degrade faster in the presence of TBA than IPA after the first hour although reductive dechlorination was inhibited by TBA. Thus, the lindane degradation process was initiated first by atomic H* dechlorination, followed by the oxidation of $^{\bullet}OH$.

In this study, H* and $^{\bullet}OH$ in the filtrate solution were very low but high in the solution with Fe-ZSM-5 (Figure 3B), suggesting Fe-ZSM-5 could stabilize and enrich the H* and $^{\bullet}OH$. Fe-ZSM-5 could also adsorb lindane (Figure S4). Less than 20% lindane of 0.8 mg/L initial concentration was adsorbed onto Fe-ZSM-5, and the equilibrium was reached in 5 min (Figure S4). About 11% of adsorbed lindane could be desorbed from Fe-ZSM-5 with DI water wash (Figure S5). Thus, the Fe-ZSM-5 surface provided a local environment where both lindane and reactive species were enriched. This is similar to the previous findings that Pd/Fe_3O_4 or Pd−In nanoparticles could be used as electron and hydrogen atom carriers facilitating the degradation of organic compounds.[30,32] XPS spectra of Fe in spent Fe-ZSM-5 became broader, and its intensity decreased(Figure S6), and the Fe concentration on the surface of spent Fe-ZSM-5 through XPS surface composition analysis decreased, showing that Fe_2O_3 was consumed and released during the electrochemical process (Table S5) and that Fe_2O_3 may be used as an active site. It was reported that Fe_2O_3 used as the active site such as in Fe_2O_3−N-doped carbon, Fe_2O_3/FeP, Fe_2O_3/NiFe-LDHs, and so forth had a better electrocatalytic performance for the HER and OER,[77−79] which usually occur during the electrolytic process.[80,81] During the HER and OER processes, H* can be generated from the reduction of water through the Volmer process (eqs 3−5),[29,82] and $^{\bullet}OH$ could be generated on the DSA anode by oxidation of water (eq 6).[83]

$$H_2O + e^- \leftrightarrow H^* + OH^- \text{—Volmer} \quad (3)$$

$$H_2O + H^* \leftrightarrow H_2 + OH^- \text{—Heyrovsky} \quad (4)$$

$$H^* + H^* \leftrightarrow H_2(g) \text{—Tafel} \quad (5)$$

$$H_2O \rightarrow {}^{\bullet}OH + H^+ + e^- \quad (6)$$

https://doi.org/10.1021/acsomega.2c04458
ACS Omega 2022, 7, 33500−33510

A total of 11 reaction intermediates including pentachlorocyclohexene (PCCH), tetrachlorocyclohexene (TeCCH), trichlorobenzene (TCB), dichlorobenzene (DCB) (including 1,2-dichlorobenzene, 1,3-dichlorobenzene, and 1,4-dichlorobenzene), chlorobenzene, 4-chlorocyclohexene, and dichlorophenol (2,4-dichlorophenol, 2,5-dichlorophenol, and 2,6-dichlorophenol) were identified by GC−MS (Figure S7). Based on this, the degradation pathway of lindane is proposed (Figure 5). With six chlorine atoms substituted, lindane is extremely electron-negative and thus resistant to oxidation. Its degradation is initiated with reductive dechlorination, generating PCCH, TeCCH, TCB, and DCB sequentially. With the decrease in the number of chlorine substitutions, the molecules became less electron-negative. When only two chlorine substitutions remained in the molecule, oxidation became possible. Thus, DCB could be oxidized to form hydroxylated products. The •OH probably played a central role in this step. Further oxidation of the molecule led to the breakdown of the ring, forming short-chain aliphatic acids such as hydracrylic acid, pyruvic acid, glyoxylic acid, and oxalate which were the last byproducts before mineralization, lowering the solution pH. This is confirmed by the final decreased pH (Figure S2).

3.5. Energy Consumption and Mineralization of Lindane. The degree of mineralization of lindane was evaluated based on the reduction of TOC (Figure 6). The mineralization efficiency of lindane increased with the current density increasing (Figure 6A). The TOC of the solution was reduced by 31.1, 50.0, 70.5, and 77.9% at the current densities of 6, 14, 20, and 30 mA/cm^2, respectively, in the presence of 0.5 g/L Fe-ZSM-5 at 8 h. The mineralization efficiency of lindane also increased with the increase of the Fe-ZSM-5 dose(Figure 6B). The TOC degradation efficiencies were 52.5, 60.7, 70.5, and 76.2% at doses of 0.1, 0.3, 0.5, and 1.0 g/L Fe-ZSM-5, respectively. EC_{TOC} increased with the increase of current densities (Figure 6C), but EC_{TOC} decreased with increasing doses of Fe-ZSM-5 (Figure 6D), showing that Fe-ZSM-5 can lower energy consumption. At 30 mA/cm^2 and 0.5 g/L Fe-ZSM-5, the EC value at hour 8 (77.9% TOC removal) was 1.2 kW h (g TOC)$^{-1}$, which was higher than the value (0.74 kW h (g TOC)$^{-1}$) at 20 mA/cm^2 (70.5% TOC removal). The EC values (<1.2 kW h (g TOC)$^{-1}$) were much lower than those reported.[12,13] Our results are similar to the recent studies that redox synergy between H* and •OH effectively lowered energy consumption and improved the degradation of persistent refractory chlorinated organic compounds.[26,84] In addition, the reusability of catalysts is crucial for practical application. To evaluate the reusability of Fe-ZSM-5, experiments were conducted by repeatedly spiking lindane to the same solution (Figure S8), and the content of Fe in ZSM-5 decreased from 0.98 to 0.56%. Fe-ZSM-5 remains highly efficient after seven cycles, indicating the excellent catalytic reusability of Fe-ZSM-5 catalysts. Thus, the Fe-ZSM-5 catalyst can be used as a promising catalyst for the degradation of lindane in an electrochemical system.

4. CONCLUSIONS

In this study, we reported a highly efficient catalytic electrochemical process consisting of commercial DSA (Ti/RuO_2−IrO_2) and graphite electrodes and Fe-ZSM-5 particles as the catalyst. Fe-ZSM-5 zeolites could stabilize and enrich the H* and •OH, and they can also enrich lindane on its surface. The degradation of lindane was initiated with the reductive dechlorination of lindane by H*, followed by •OH oxidation that led to the cleavage of the ring ultimately. Fe-ZSM-5 significantly accelerated lindane degradation and reduced energy consumption. These results are valuable for the design and application of synthetic iron-loaded catalysts for the reduction−oxidation of organochlorine compounds in electrochemical processes.

■ ASSOCIATED CONTENT

Supporting Information

The Supporting Information is available free of charge at https://pubs.acs.org/doi/10.1021/acsomega.2c04458.

Experimental section; surface area and pore volumes of Fe-ZSM-5; atomic percentage of O, Al, Si, and Fe in ZSM-5 and Fe-ZSM-5; degradation kinetics of lindane under different conditions in the presence of Fe-ZSM-5 zeolites; degradation kinetics of lindane under different conditions in the absence of Fe-ZSM-5 zeolites; surface elements of fresh and spent Fe-ZSM-5; characteristic of ZSM-5 and Fe-ZSM-5; final pH in the solution after reaction 8 h in the presence of Fe-ZSM-5; lindane removal with three scavengers; adsorption−desorption of lindane; XPS spectra of spent Fe-ZSM-5; and intermediates of lindane degradation (PDF)

■ AUTHOR INFORMATION

Corresponding Author

Yun Liu − *Key Laboratory of Soil Environment and Pollution Remediation, Institute of Soil Science, Chinese Academy of Sciences, Nanjing 210008, China; University of Chinese Academy of Sciences, Beijing 100000, China;* orcid.org/0000-0002-7320-5766; Email: yliu@issas.ac.cn

Authors

Yuexuan Li − *Key Laboratory of Soil Environment and Pollution Remediation, Institute of Soil Science, Chinese Academy of Sciences, Nanjing 210008, China; Lanzhou Jiaotong University, Lanzhou 730070, China*

Xuan Zhang − *Lanzhou Jiaotong University, Lanzhou 730070, China*

Kun Tian − *Key Laboratory of Soil Environment and Pollution Remediation, Institute of Soil Science, Chinese Academy of Sciences, Nanjing 210008, China; University of Chinese Academy of Sciences, Beijing 100000, China*

Ding Tan − *Key Laboratory of Soil Environment and Pollution Remediation, Institute of Soil Science, Chinese Academy of Sciences, Nanjing 210008, China; University of Chinese Academy of Sciences, Beijing 100000, China*

Xiaosan Song − *Lanzhou Jiaotong University, Lanzhou 730070, China*

Ping Wang − *Lanzhou Jiaotong University, Lanzhou 730070, China*

Qian Jiang − *Key Laboratory of Soil Environment and Pollution Remediation, Institute of Soil Science, Chinese Academy of Sciences, Nanjing 210008, China*

Junhe Lu − *College of Resources and Environmental Science, Nanjing Agricultural University, Nanjing 210095, China;* orcid.org/0000-0001-6068-5820

Complete contact information is available at: https://pubs.acs.org/10.1021/acsomega.2c04458

Notes

The authors declare no competing financial interest.

https://doi.org/10.1021/acsomega.2c04458
ACS Omega 2022, 7, 33500−33510

■ ACKNOWLEDGMENTS

This work was supported by the National Key Research and Development Program of China (2020YFC1807200), the National Natural Science Foundation of China (41877504), and the Open Fund of National Engineering Laboratory for Site Remediation Technologies (NEL-SRT201902).

■ REFERENCES

(1) Zhang, J.; Lei, C.; Chen, W.; Xie, Q.; Guo, Q.; Huang, B. Electrochemical-driven nanoparticulate catalysis for highly efficient dechlorination of chlorinated environmental pollutant. *J. Catal.* **2021**, *395*, 362−374.
(2) Arellano-González, M. Á.; González, I.; Texier, A.C. Mineralization of 2-chlorophenol by sequential electrochemical reductive dechlorination and biological processes. *J. Hazard. Mater.* **2016**, *314*, 181−187.
(3) Yin, H.; Cao, X.; Lei, C.; Chen, W.; Huang, B. Insights into electroreductive dehalogenation mechanisms of chlorinated environmental pollutants. *ChemElectroChem* **2020**, *7*, 1825−1837.
(4) Li, Y. F. Global technical hexachlorocyclohexane usage and its contamination consequences in the environment: from 1948 to 1997. *Sci. Total Environ.* **1999**, *232*, 121−158.
(5) Chang, C.; Lian, F.; Zhu, L. Simultaneous adsorption and degradation of gamma-HCH by nZVI/Cu bimetallic nanoparticles with activated carbon support. *Environ. Pollut.* **2011**, *159*, 2507−2514.
(6) Walker, K.; Vallero, D. A.; Lewis, R. G. Factors influencing the distribution of lindane and other hexachlorocyclohexanes in the environment. *Environ. Sci. Technol.* **1999**, *33*, 4373−4378.
(7) Lorenzo, D.; García-Cervilla, R.; Romero, A.; Santos, A. Partitioning of chlorinated organic compounds from dense non-aqueous phase liquids and contaminated soils from lindane production wastes to the aqueous phase. *Chemosphere* **2020**, *239*, 124798.
(8) Vijgen, J.; de Borst, B.; Weber, R.; Stobiecki, T.; Forter, M. HCH and lindane contaminated sites: European and global need for a permanent solution for a long-time neglected issue. *Environ. Pollut.* **2019**, *248*, 696−705.
(9) Cuozzo, S. A.; Sineli, P. E.; Davila Costa, J. D.; Tortella, G. Streptomyces sp is a powerful biotechnological tool for the biodegradation of HCH isomers: Biochemical and molecular basis. *Crit. Rev. Biotechnol.* **2018**, *38*, 719−728.
(10) Wacławek, S.; Silvestri, D.; Hrabák, P.; Padil, V. V.; Torres-Mendieta, R.; Wacławek, M.; Černík, M.; Dionysiou, D. D. Chemical oxidation and reduction of hexachlorocyclohexanes: A review. *Water Res.* **2019**, *162*, 302−319.
(11) Cheng, M.; Zeng, G. M.; Huang, D. L.; Lai, C.; Xu, P.; Zhang, C.; Liu, Y. Hydroxyl radicals based advanced oxidation processes (AOPs) for remediation of soils contaminated with organic compounds: A review. *Chem. Eng. J.* **2016**, *284*, 582−598.
(12) Dominguez, C. M.; Oturan, N.; Romero, A.; Santos, A.; Oturan, M. A. Optimization of electro-Fenton process for effective degradation of organochlorine pesticide lindane. *Catal. Today* **2018**, *313*, 196−202.
(13) Dominguez, C. M.; Oturan, N.; Romero, A.; Santos, A.; Oturan, M. A. Lindane degradation by electrooxidation process: Effect of electrode materials on oxidation and mineralization kinetics. *Water Res.* **2018**, *135*, 220−230.
(14) Ganiyu, S. O.; Zhou, M.; Martínez-Huitle, C. A. Heterogeneous electro-Fenton and photoelectro-Fenton processes: A critical review of fundamental principles and application for water/wastewater treatment. *Appl. Catal., B* **2018**, *235*, 103−129.
(15) Cao, P.; Quan, X.; Zhao, K.; Chen, S.; Yu, H.; Niu, J. Selective electrochemical H_2O_2 generation and activation on a bifunctional catalyst for heterogeneous electro-Fenton catalysis. *J. Hazard. Mater.* **2020**, *382*, 121102.
(16) Zahrani, A. A.; Ayati, B. Improving Fe-based heterogeneous Electro-Fenton nano catalyst using transition metals in a novel orbiting electrodes reactor. *Chemosphere* **2020**, *256*, 127049.
(17) Poza-Nogueiras, V.; Rosales, E.; Pazos, M.; Sanromán, M. A. Current advances and trends in electro-Fenton process using heterogeneous catalysts - A review. *Chemosphere* **2018**, *201*, 399−416.
(18) Ghasemi, M.; Khataee, A.; Gholami, P.; Soltani, R. D. Template-free microspheres decorated with Cu-Fe-NLDH for catalytic removal of gentamicin in heterogeneous electro-Fenton process. *J. Environ. Manage.* **2019**, *248*, 109236.
(19) Rache, M. L.; García, A. R.; Zea, H. R.; Silva, A. M.; Madeira, L. M.; Ramírez, J. H. Azo-dye orange II degradation by the heterogeneous Fenton-like process using a zeolite Y-Fe catalyst—kinetics with a model based on the Fermi's equation. *Appl. Catal., B* **2014**, *146*, 192−200.
(20) Özcan, A.; Atılır Özcan, A. A.; Demirci, Y.; Şener, E. Preparation of Fe_2O_3 modified kaolin and application in heterogeneous electro-catalytic oxidation of enoxacin. *Appl. Catal., B* **2017**, *200*, 361−371.
(21) Sadeghi, M.; Mehdinejad, M. H.; Mengelizadeh, N.; Mahdavi, Y.; Pourzamani, H.; Hajizadeh, Y.; Zare, M. R. Degradation of diclofenac by heterogeneous electro-Fenton process using magnetic single-walled carbon nanotubes as a catalyst. *J. Water Proc. Eng.* **2019**, *31*, 100852.
(22) Dominguez, C. M.; Parchão, J.; Rodriguez, S.; Lorenzo, D.; Romero, A.; Santos, A. Kinetics of lindane dechlorination by zerovalent iron microparticles: Effect of different salts and stability study. *Ind. Eng. Chem. Res.* **2016**, *55*, 12776−12785.
(23) San Román, I.; Galdames, A.; Alonso, M.; Bartolomé, L.; Vilas, J.; Alonso, R. Effect of coating on the environmental applications of zero valent iron nanoparticles: The lindane case. *Sci. Total Environ.* **2016**, *565*, 795−803.
(24) Joo, S. H.; Zhao, D. Destruction of lindane and atrazine using stabilized iron nanoparticles under aerobic and anaerobic conditions: Effects of catalyst and stabilizer. *Chemosphere* **2008**, *70*, 418−425.
(25) Wang, C.W.; Chang, S.C.; Liang, C. Persistent organic pollutant lindane degradation by alkaline cold-brew green tea. *Chemosphere* **2019**, *232*, 281−286.
(26) Zhang, J.; Ji, Q.; Lan, H.; Zhang, G.; Liu, H.; Qu, J. Synchronous reduction-oxidation process for efficient removal of trichloroacetic acid: H* initiates dechlorination and ·OH is responsible for removal efficiency. *Environ. Sci. Technol.* **2019**, *53*, 14586−14594.
(27) Nagpal, V.; Bokare, A. D.; Chikate, R. C.; Rode, C. V.; Paknikar, K. M. Reductive dechlorination of γ-hexachlorocyclohexane using Fe−Pd bimetallic nanoparticles. *J. Hazard. Mater.* **2010**, *175*, 680−687.
(28) Mao, R.; Huang, C.; Zhao, X.; Ma, M.; Qu, J. H. Dechlorination of triclosan by enhanced atomic hydrogen-mediated electrochemical reduction: Kinetics, mechanism, and toxicity assessment. *Appl. Catal., B* **2019**, *241*, 120−129.
(29) Mao, R.; Lan, H.; Yan, L.; Zhao, X.; Liu, H.; Qu, J. Enhanced indirect atomic H* reduction at a hybrid Pd/graphene cathode for electrochemical dechlorination under low negative potentials. *Environ. Sci.: Nano* **2018**, *5*, 2282−2292.
(30) Zhou, Y. J.; Zhang, G.; Ji, Q. H.; Zhang, W.; Zhang, J. Y.; Liu, H. J.; Qu, J. H. Enhanced stabilization and effective utilization of atomic hydrogen on Pd-In nanoparticles in a flow-through electrode. *Environ. Sci. Technol.* **2019**, *53*, 11383−11390.
(31) Wu, Y.; Gan, L.; Zhang, S.; Song, H.; Lu, C.; Li, W.; Wang, Z.; Jiang, B.; Li, A. Carbon-nanotube-doped Pd-Ni bimetallic three-dimensional electrode for electrocatalytic hydrodechlorination of 4-chlorophenol: Enhanced activity and stability. *J. Hazard. Mater.* **2018**, *356*, 17−25.
(32) Mao, R.; Li, N.; Lan, H.; Zhao, X.; Liu, H.; Qu, J.; Sun, M. Dechlorination of trichloroacetic acid using a noble metal-free graphene−Cu foam electrode via direct cathodic reduction and atomic H. *Environ. Sci. Technol.* **2016**, *50*, 3829−3837.
(33) Jiang, G.; Lan, M.; Zhang, Z.; Lv, X.; Lou, Z.; Xu, X.; Dong, F.; Zhang, S. Identification of active hydrogen species on Palladium nanoparticles for an enhanced electrocatalytic hydrodechlorination of

https://doi.org/10.1021/acsomega.2c04458
ACS Omega 2022, 7, 33500−33510

2,4-dichlorophenol in water. *Environ. Sci. Technol.* **2017**, *51*, 7599−7605.
(34) Xu, D.; Zhang, L.; Wang, H.; Bian, Z. Optimization of electrochemical sequential reduction-oxidation of chlorophene with CoNi alloy anchored ionic liquid-graphene cathode: Comparison, mechanism and toxicity study. *Chem. Eng. J.* **2019**, *358*, 1371−1382.
(35) Li, Y.; Miller, C. J.; Wu, L.; Waite, T. D. Hydroxyl radical production via a reaction of electrochemically generated hydrogen peroxide and atomic hydrogen: An effective process for contaminant oxidation? *Environ. Sci. Technol.* **2022**, *56*, 5820−5829.
(36) Muthurasu, A.; Maruthapandian, V.; Kim, H. Y. Metal-organic framework derived Co_3O_4/MoS_2 heterostructure for efficient bifunctional electrocatalysts for oxygen evolution reaction and hydrogen evolution reaction. *Appl. Catal., B* **2019**, *248*, 202−210.
(37) Henke, A. H.; Saunders, T. P.; Pedersen, J. A.; Hamers, R. J. Enhancing electrochemical efficiency of hydroxyl radical formation on diamond electrodes by functionalization with hydrophobic monolayers. *Langmuir* **2018**, *35*, 2153−2163.
(38) Kasahara, S.; Natsui, K.; Watanabe, T.; Yokota, Y.; Kim, Y.; Iizuka, S.; Tateyama, Y.; Einaga, Y. Surface hydrogenation of boron-doped diamond electrodes by cathodic reduction. *Anal. Chem.* **2017**, *89*, 11341−11347.
(39) Abdalrhman, A. S.; Gamal El-Din, M. G. Degradation of organics in real oil sands process water by electro-oxidation using graphite and dimensionally stable anodes. *Chem. Eng. J.* **2020**, *389*, 124406.
(40) Brillas, E. Progress of homogeneous and heterogeneous electro-Fenton treatments of antibiotics in synthetic and real wastewaters. A critical review on the period 2017-2021. *Sci. Total Environ.* **2022**, *819*, 153102.
(41) Raghu, S.; Ahmed Basha, C. Dye destruction and simultaneous generation of sodium hydroxide using a divided electrochemical reactor. *Ind. Eng. Chem. Res.* **2008**, *47*, 5277−5283.
(42) Wang, Z.; Teng, X.; Xie, M.; Cheng, X.; Li, J. Pretreatment of polyvinyl alcohol by electrocoagulation coupling with catalytic oxidation: Performance, mechanism and pathway. *Chin. Chem. Lett.* **2020**, *31*, 2864−2870.
(43) Ren, G.; Zhou, M.; Zhang, Q.; Xu, X.; Li, Y.; Su, P.; Paidar, M.; Bouzek, K. Cost-efficient improvement of coking wastewater biodegradability by multi-stages flow through peroxi-coagulation under low current load. *Water Res.* **2019**, *154*, 336−348.
(44) Wang, W.; Wang, X. Investigation of Ir-modified carbon felt as the positive electrode of an all-vanadium redox flow battery. *Electrochim. Acta* **2007**, *52*, 6755−6762.
(45) Linnemann, J.; Kanokkanchana, K.; Tschulik, K. Design strategies for electrocatalysts from an electrochemist's perspective. *ACS Catal.* **2021**, *11*, 5318−5346.
(46) Zhang, W.; Ye, W.; Hu, X.; Liang, W. Electrocatalytic degradation of humic acid using particle electrodes of activated carbon loaded with metallic cobalt. *Chemosphere* **2021**, *263*, 128200.
(47) Zeng, H.; Zhao, X.; Zhao, F.; Park, Y.; Sillanpää, M. Accelerated Fe^{3+}/Fe^{2+} cycle using atomic H* on Pd/Al_2O_3: A novel mechanism for an electrochemical system with particle electrode for iron sludge reduction in the Fe^{2+}/peroxydisulfate oxidation process. *Chem. Eng. J.* **2020**, *382*, 122972.
(48) Li, J.; Yan, J.; Yao, G.; Zhang, Y.; Li, X.; Lai, B. Improving the degradation of atrazine in the three-dimensional (3D) electrochemical process using $CuFe_2O_4$ as both particle electrode and catalyst for persulfate activation. *Chem. Eng. J.* **2019**, *361*, 1317−1332.
(49) Zhu, Y.; Lin, Q.; Zhong, Y.; Tahini, H. A.; Shao, Z.; Wang, H. Metal oxide-based materials as an emerging family of hydrogen evolution electrocatalysts. *Energy Environ. Sci.* **2020**, *13*, 3361−3392.
(50) Yan, Y.; Jiang, S. S.; Zhang, H. P.; Zhang, X. Y. Preparation of novel Fe-ZSM-5 zeolite membrane catalysts for catalytic wet peroxide oxidation of phenol in a membrane reactor. *Chem. Eng. J.* **2015**, *259*, 243−251.
(51) Sheng-tao, J.; Zhu, J. Z.; Bai, S. L.; Guan, Y. J.; Yao, J. Research on Fe-loaded ZSM-5 molecular sieve catalyst in high-concentration aniline wastewater treatment. *Desalin. Water Treat.* **2016**, *57*, 791−798.
(52) Ou, X. X.; Pilitsis, F.; Jiao, Y. L.; Zhang, Y.; Xu, S. J.; Jennings, M.; Yang, Y.; Taylor, S. F. R.; Garforth, A.; Zhang, H. P.; et al. Hierarchical Fe-ZSM-5/SiC foam catalyst as the foam bed catalytic reactor (FBCR) for catalytic wet peroxide oxidation (CWPO). *Chem. Eng. J.* **2019**, *362*, 53−62.
(53) Velichkova, F.; Delmas, H.; Julcour, C.; Koumanova, B. Heterogeneous fenton and photo-fenton oxidation for paracetamol removal using iron containing ZSM-5 zeolite as catalyst. *AIChE J.* **2017**, *63*, 669−679.
(54) Cihanoğlu, A.; Gündüz, G.; Dükkancı, M. Degradation of acetic acid by heterogeneous Fenton-like oxidation over iron-containing ZSM-5 zeolites. *Appl. Catal., B* **2015**, *165*, 687−699.
(55) Sashkina, K. A.; Parkhomchuk, E. V.; Rudina, N. A.; Parmon, V. N. The role of zeolite Fe-ZSM-5 porous structure for heterogeneous Fenton catalyst activity and stability. *Micropor. Mesopor. Mater.* **2014**, *189*, 181−188.
(56) Rodeghero, E.; Martucci, A.; Cruciani, G.; Bagatin, R.; Sarti, E.; Bosi, V.; Pasti, L. Kinetics and dynamic behaviour of toluene desorption from ZSM-5 using in situ high-temperature synchrotron powder X-ray diffraction and chromatographic techniques. *Catal. Today* **2016**, *277*, 118−125.
(57) Bai, Y.; Zhang, G.; Liu, D.; Zhang, Y.; Zhao, L.; Gao, J.; Xu, C.; Meng, Q.; Gao, X. The advance in catalytic pyrolysis of naphtha technology using ZSM-5 as catalyst. *Appl. Catal., A* **2021**, *628*, 118399.
(58) Zhang, S.; Yang, M.; Shao, J.; Yang, H.; Zeng, K.; Chen, Y.; Luo, J.; Agblevor, F. A.; Chen, H. The conversion of biomass to light olefins on Fe-modified ZSM-5 catalyst: Effect of pyrolysis parameters. *Sci. Total Environ.* **2018**, *628*−*629*, 350−357.
(59) Huang, P.; Lei, J.; Sun, Z.; Hu, X. Fabrication of MOF-derivated CuOx-C electrode for electrochemical degradation of ceftazidime from aqueous solution. *Chemosphere* **2021**, *268*, 129157.
(60) Othman, I.; Hisham Zain, J. H.; Abu Haija, M. A.; Banat, F. Catalytic activation of peroxymonosulfate using $CeVO_4$ for phenol degradation: an insight into the reaction pathway. *Appl. Catal., B* **2020**, *266*, 118601.
(61) Chen, J.; Xia, Y.; Dai, Q. Electrochemical degradation of chloramphenicol with a novel Al doped PbO_2 electrode: Performance, kinetics and degradation mechanism. *Electrochim. Acta* **2015**, *165*, 277−287.
(62) Zhang, Y.; Chen, Z.; Zhou, L.; Wu, P.; Zhao, Y.; Lai, Y.; Wang, F.; Li, S. Efficient electrochemical degradation of tetrabromobisphenol A using MnO_2/MWCNT composites modified Ni foam as cathode: Kinetic analysis, mechanism and degradation pathway. *J. Hazard. Mater.* **2019**, *369*, 770−779.
(63) Barhoumi, N.; Olvera-Vargas, H.; Oturan, N.; Huguenot, D.; Gadri, A.; Ammar, S.; Brillas, E.; Oturan, M. A. Kinetics of oxidative degradation/mineralization pathways of the antibiotic tetracycline by the novel heterogeneous electro-Fenton process with solid catalyst chalcopyrite. *Appl. Catal., B* **2017**, *209*, 637−647.
(64) Zhang, J.; Qiu, S.; Feng, H.; Hu, T.; Wu, Y.; Luo, T.; Tang, W.; Wang, D. Efficient degradation of tetracycline using core−shell Fe@Fe_2O_3-CeO_2 composite as novel heterogeneous electro-Fenton catalyst. *Chem. Eng. J.* **2022**, *428*, 131403.
(65) Zhang, L.; Lin, Y. Facile synthesis of N-doped carbon supported iron species for highly efficient methane conversion with H_2O_2 at ambient temperature. *Appl. Catal., A* **2021**, *615*, 118052.
(66) Xie, J.; Jin, R.; Li, A.; Bi, Y.; Ruan, Q.; Deng, Y.; Zhang, Y.; Yao, S.; Sankar, G.; Ma, D.; Tang, J. Highly selective oxidation of methane to methanol at ambient conditions by titanium dioxide-supported iron species. *Nat. Catal.* **2018**, *1*, 889−896.
(67) Meng, L.; Zhu, X.; Hensen, E. J. Stable Fe/ZSM-5 nanosheet zeolite catalysts for the oxidation of benzene to phenol. *ACS Catal.* **2017**, *7*, 2709−2719.
(68) Gu, Y.; Chen, P.; Wang, X.; Lyu, Y.; Liu, W.; Liu, X.; Yan, Z. Active sites and induction period of Fe/ZSM-5 catalyst in methane dehydroaromatization. *ACS Catal.* **2021**, *11*, 6771−6786.

https://doi.org/10.1021/acsomega.2c04458
ACS Omega 2022, 7, 33500−33510

(69) Sun, K.; Xia, H.; Feng, Z.; Vansanten, R.; Hensen, E.; Li, C. Active sites in Fe/ZSM-5 for nitrous oxide decomposition and benzene hydroxylation with nitrous oxide. *J. Catal.* **2008**, *254*, 383−396.
(70) Schwidder, M.; Kumar, M. S.; Klementiev, K.; Pohl, M. M.; Bruckner, A.; Grunert, W. Selective reduction of NO with Fe-ZSM-5 catalysts of low Fe content: I. Relations between active site structure and catalytic performance. *J. Catal.* **2005**, *231*, 314−330.
(71) Mao, R.; Zhao, X.; Lan, H.; Liu, H.; Qu, J. Efficient electrochemical reduction of bromate by a Pd/rGO/CFP electrode with low applied potentials. *Appl. Catal., B* **2014**, *160-161*, 179−187.
(72) Zhao, Q.; Fang, Q.; Liu, H.; Li, Y.; Cui, H.; Zhang, B.; Tian, S. Halide-specific enhancement of photodegradation for sulfadiazine in estuarine waters: Roles of halogen radicals and main water constituents. *Water Res.* **2019**, *160*, 209−216.
(73) Buxton, G. V.; Greenstock, C. L.; Helman, W. P.; Ross, A. B. Critical review of rate constants for reactions of hydrated electrons, hydrogen atoms and hydroxyl radicals (·OH/·O^- in aqueous solution. *J. Phys. Chem. Ref. Data* **1988**, *17*, 513−886.
(74) Muñoz-Morales, M.; Sáez, C.; Cañizares, P.; Rodrigo, M. A. Enhanced electrolytic treatment for the removal of clopyralid and lindane. *Chemosphere* **2019**, *234*, 132−138.
(75) de Santana Mota, W. J.; Santos, G. O. S.; Resende Dória, A. R.; Rubens dos Reis Souza, M. R.; Krause, L. C.; Salazar-Banda, G. R.; Barrios Eguiluz, K. I. B.; López, J. A.; Hernández-Macedo, M. L. Enhanced HCB removal using bacteria from mangrove as post-treatment after electrochemical oxidation using a laser-prepared Ti/RuO_2−IrO_2−TiO_2 anode. *Chemosphere* **2021**, *279*, 130875.
(76) Dominguez, C. M.; Oturan, N.; Romero, A.; Santos, A.; Oturan, M. A. Removal of lindane wastes by advanced electrochemical oxidation. *Chemosphere* **2018**, *202*, 400−409.
(77) Jiang, J.; Zhu, L.; Sun, Y.; Chen, Y.; Chen, H.; Han, S.; Lin, H. Fe_2O_3 nanocatalysts on N-doped carbon nanomaterial for highly efficient electrochemical hydrogen evolution in alkaline. *J. Power Sources* **2019**, *426*, 74−83.
(78) Li, C.-F.; Xie, L.J.; Zhao, J.W.; Gu, L.F.; Wu, J.Q.; Li, G.R. Interfacial electronic modulation by Fe_2O_3/NiFe-LDHs heterostructures for efficient oxygen evolution at high current density. *Appl. Catal., B* **2022**, *306*, 121097.
(79) Ahmad, I.; Ahmed, J.; Batool, S.; Zafar, M. N.; Hanif, A.; Zahidullah, M. F.; Nazar, A.; Ul-Hamid, U.; Jabeen, A.; Dahshan, M.; Idrees, M.; Shehzadi, S. A. Design and fabrication of Fe_2O_3/FeP heterostructure for oxygen evolution reaction electrocatalysis. *J. Alloys Compd.* **2022**, *894*, 162409.
(80) Dotan, H.; Landman, A.; Sheehan, S. W.; Malviya, K. D.; Shter, G. E.; Grave, D. A.; Arzi, Z.; Yehudai, N.; Halabi, M.; Gal, N.; Hadari, N.; Cohen, C.; Rothschild, A.; Grader, G. S. Decoupled hydrogen and oxygen evolution by a two-step electrochemical−chemical cycle for efficient overall water splitting. *Nat. Energy* **2019**, *4*, 786−795.
(81) Yu, J.; He, Q.; Yang, G.; Zhou, W.; Shao, Z.; Ni, M. Recent advances and prospective in ruthenium-based materials for electrochemical water splitting. *ACS Catal.* **2019**, *9*, 9973−10011.
(82) Li, A. Z.; Zhao, X.; Hou, Y. N.; Liu, H. J.; Wu, L. Y.; Qu, J. H. The electrocatalytic dechlorination of chloroacetic acids at electrodeposited Pd/Fe-modified carbon paper electrode. *Appl. Catal., B* **2012**, *111−112*, 628−635.
(83) Espinoza, L. C.; Sepúlveda, P.; García, A.; Martins de Godoi, D. M.; Salazar, R. Degradation of oxamic acid using dimensionally stable anodes (DSA) based on a mixture of RuO_2 and IrO_2 nanoparticles. *Chemosphere* **2020**, *251*, 126674.
(84) Zhang, J.; Zhang, G.; Lan, H.; Qu, J.; Liu, H. Synergetic hydroxyl radical oxidation with atomic hydrogen reduction lowers the organochlorine conversion barrier and potentiates effective contaminant mineralization. *Environ. Sci. Technol.* **2021**, *55*, 3296−3304.

https://doi.org/10.1021/acsomega.2c04458
ACS Omega 2022, 7, 33500−33510